AIAA SciTech Forum
8-12 January 2024, Orlando, FL
AIAA SCITECH 2024 Forum

10.2514/6.2024-0249

Domain-Decomposed Reduced Order Modelling of Transonic Airfoil Flow with Transported Snapshot Approach

Navdeep Pandey* and Aniruddha Sinha†
Dept. of Aerospace Engineering, Indian Institute of Technology Bombay, Mumbai, 400076, INDIA

High-fidelity CFD computations are challenging because of their high computational cost and turn-around time, so that one cannot rely solely on them in preliminary design phases. Researchers have been working on various model-order reduction (MOR) techniques to alleviate this issue, but transonic aerodynamics problems remain a challenge. We propose a novel MOR technique for steady transonic flow characterized by parameter-dependent discontinuities. It is a combination of transported snapshot MOR (TSMOR) and reduced order model based on proper orthogonal decomposition (POD-ROM). The overall idea is to decompose the whole domain into two sub-domains, perform TSMOR in the discontinuous flow sub-domain and POD-ROM in the continuous flow one, and match the two solutions at the interface. Encouraging results are reported here for a transonic (2D) airfoil problem.

I. Introduction

Computational fluid dynamics (CFD) has become the main tool for analyzing flow problems, having applications in most of the engineering streams. Recent advancements in computer algorithms and architecture have paved the way for very efficient CFD analysis. In most areas of research, CFD simulation is supplanting experimental analysis due to its relative economy and time efficiency. However, high-fidelity CFD simulations are still challenging for industry-relevant problems involving realistic complex geoemetry. Hence, one cannot employ CFD as a tool in fields where rapid design decisions have to be made, such as in multidisciplinary optimization and control. The fundamental reason for such high computational and time expense is the high degree of freedom (DOF) that comes from the spatial discretization of the domain (or particle discretization in case of meshless methods). Researchers have been working to circumvent this bottleneck by somehow decreasing the DOF associated with the problem – an approach called model order reduction (MOR); the present work proposes a new kind of MOR.

The prevalent MOR techniques are projection based, where state variables are approximated as a linear combination of a reduced-order basis (ROB) spanning a low-dimensional sub-space. There are several tools available for extracting these ROB – e.g., proper orthogonal decomposition (POD), dynamic mode decomposition (DMD), etc. There has been significant progress in developing MORs for subsonic aerodynamics, where POD-based reduced order model (POD-ROM) is the most widely used approach. However, application to transonic and supersonic aerodynamics remains unresolved due to the challenge faced by projection-based MORs in handling time-dependent or parameter-dependent moving shocks. Several attempts have been made to tackle this problem using various specific strategies [1–4]. Transported snapshot MOR (TSMOR) is one such technique proposed by Nair and Balajewicz [5] for the prediction of shock-dominated flow fields. Although TSMOR has demonstrated promise in simple problems [5, 6], its applicability to cases with non-trivial geometries remains an open question. In the present work on reduced-order modelling of transonic airfoil flow, we present a novel approach that marries the POD-ROM approach with TSMOR in a domain-decomposed setting, leveraging their different strengths in their respective zones of applicability.

The overall objective of this work is to efficiently predict the flow field around an airfoil in a transonic flow regime under different operating conditions (i.e., freestream Mach number M_∞ and angle of attack α) by implementing TSMOR and POD-ROM in a domain-decomposed approach. Since POD-ROM is incapable of accurately predicting the flow field solution in the presence of shocks, the whole flow domain Ω has been divided into two sub-domains – shock wave Ω_d and smooth Ω_c. TSMOR and POD-ROM are respectively employed to predict the flow field in the Ω_d and Ω_c sub-domains. In TSMOR, neighbouring snapshots are transported to serve as spatial basis functions and the flow solution is reconstructed as a linear combination of such basis functions. Because of the transport, this constitutes a nonlinear MOR; the final flow solution is a nonlinear function of the input flow solutions at neighbouring parameter values. On the other hand, in the linear POD-ROM approach, POD is used to arrive at the spatial basis functions.

*Graduate student; AIAA Student Member
†Associate Professor; AIAA Member; Corresponding author: sinha.a@iitb.ac.in

For both TSMOR and POD-ROM techniques, the generalized coordinates (i.e., coefficients of basis functions) in the reconstruction of the solution are determined by minimizing the residual computed over the entire domain or some part of it (the latter strategy is called hyper-reduction). The flow solutions in the Ω_d and Ω_c sub-domains are matched at their interface through a few iterations of the TSMOR and POD-ROM calculations. The number of generalized coordinates that need to be calculated is typically very small ($O(10)$). Moreover, hyper-reduction reduces the cost of evaluation of the residual drastically without significant degradation of accuracy. Thus, the proposed method is expected to yield a drastic decrease in the overall computational effort and time consumed when compared to the prevailing full-order CFD analysis, while having minimal impact on fidelity. Recently, we have proposed a similar domain-decomposed approach but for *subsonic* store-separation trajectory prediction [7, 8].

This abstract presents preliminary results from this approach. Specifically, we show the action of the algorithm to automatically mark off the Ω_d sub-domain (and, by exclusion, the Ω_c one). Moreover, we demonstrate the implementation of the first part of the TSMOR method in Ω_d. Results from the complete implementation of TSMOR and POD-ROM integrated in the domain-decomposed setting will be presented in the final paper.

II. Theory

We will start by describing the POD-ROM approach in section II.A that applies to shock-free (i.e., smooth flow) regions, followed by the TSMOR technique in section II.B that is suited for the shock-dominated regions. Finally, section II.C will present the domain-decomposed approach that brings together POD-ROM and TSMOR to efficiently solve a typical flow problem where small regions are dominated by shocks within a much larger smooth flow domain.

A. POD-ROM

As in most MORs, this approach too has a one-time expensive 'offline' stage wherein a rich database is generated and the POD basis is calculated therefrom, followed by a many-query inexpensive 'online' stage.

1. Offline stage

Let $\{\boldsymbol{q}(\boldsymbol{x};\boldsymbol{\mu}_j)\}_{j=1}^{N_s}$ represent a set of N_s vector fields of relevant flow variables in a steady problem. For the two-dimensional flows considered here, $\boldsymbol{x} := (x, y)$ in Cartesian coordinates. In case of a 2D problem, $\boldsymbol{q}$ may be $[\rho, \rho u, \rho v, p]^{\mathrm{T}}$, where ρ is the density, u & v are the x- & y-components of velocity respectively, and p is the pressure. Moreover, $\boldsymbol{\mu}$ is the vector of operating parameters; e.g., $\boldsymbol{\mu} = [M_\infty, \alpha]^{\mathrm{T}}$ in a 2D airfoil problem, with M_∞ and α being respectively the freestream Mach number and airfoil angle of attack. We assume that the flow fields (called 'snapshots' hereafter) available in the learning database (as well as the unsampled ones lying in their parameter range) may subscribe to an efficient approximate affine linear modal decomposition such that

$$\boldsymbol{q}(\boldsymbol{x};\boldsymbol{\mu}) \approx \overline{\boldsymbol{q}}(\boldsymbol{x}) + \sum_{n=1}^{N_p} \eta^{(n)}(\boldsymbol{\mu})\widetilde{\boldsymbol{q}}^{(n)}(\boldsymbol{x}). \tag{1}$$

Here, $\overline{\boldsymbol{q}}$ represents the base flow variable vector field, which is typically obtained by averaging across all the snapshots of the learning database. The deviation of each solution (snapshot) from the base flow is assumed to be well approximated by a linear combination of N_p spatial 'modes' (or basis flow fields) $\{\widetilde{\boldsymbol{q}}^{(n)}(\boldsymbol{x})\}_{n=1}^{N_p}$ weighted by the coefficients $\{\eta^{(n)}(\boldsymbol{\mu})\}_{n=1}^{N_p}$. For an efficient order reduction, N_p is typically much smaller than the number of grid points needed to represent the flow domain for a converged numerical simulation. For convenience, we will write the vector of weight coefficients as $\boldsymbol{\eta}(\boldsymbol{\mu}) := (\eta^{(1)}(\boldsymbol{\mu}), \eta^{(2)}(\boldsymbol{\mu}), \ldots, \eta^{(N_p)}(\boldsymbol{\mu}))^{\mathrm{T}}$. In this work, the above basis flow fields are obtained using the very well-established approach of POD [9, 10], wherein the bases $\widetilde{\boldsymbol{q}}^{(n)}$ are ordered by their decreasing prevalence in the database given by the respective POD eigenvalues $\lambda^{(n)}$. For brevity, we omit the details here; further discussion of the variant of POD that is most relevant for the present work has been described by Sinha et al. [11].

2. Online stage

The (approximate) prediction of the flow field for a new parameter vector outside the learning database, say $\boldsymbol{\mu}_0$, is pursued using reduced-order modelling (ROM) in the online stage. Rather than simply interpolating the parameter space, a more robust and accurate approach is to invoke the underlying governing equations of the flow, or a simplification thereof. It is based on the reduced order modal decomposition of the flow field, i.e., the POD. Equation (1) reveals that

this comes down to determining the new set of (POD) coefficients $\boldsymbol{\eta}(\boldsymbol{\mu}_0)$. The basic methodology of POD-based ROM was proposed in Ref. [12], which was further refined over the subsequent years [11, 13, 14].

Let the full order model (FOM) steady flow problem be represented by

$$\boldsymbol{R}(\boldsymbol{q}(\boldsymbol{x};\boldsymbol{\mu})) = 0 \quad \forall \boldsymbol{x} \in \Omega, \qquad \text{subject to} \quad \boldsymbol{B}(\boldsymbol{q}(\boldsymbol{x};\boldsymbol{\mu})) = 0 \quad \forall \boldsymbol{x} \in \delta. \tag{2}$$

Here, $\boldsymbol{R}(\boldsymbol{q})$ is the 'residual' of the governing equations, and Ω represents the relevant flow domain. For example, in 2D inviscid flows, $\boldsymbol{R}$ is a four-dimensional vector corresponding to the equations encoding conservation of mass, two components of momentum and energy. Moreover, $\boldsymbol{B}$ represents the vector of functions that have to be zeroed at a part or the whole of the boundary of the flow domain δ – the boundary conditions.

In the POD-based ROM, we substitute the approximate expansion of eqn. (1) in the above governing equations. Since the base flow field and the POD modes are known from the learning database, the residual and boundary conditions are now approximated as $\boldsymbol{R}(\boldsymbol{q}(\boldsymbol{x};\boldsymbol{\mu}_0)) \approx \tilde{\boldsymbol{R}}(\boldsymbol{x};\boldsymbol{\eta}(\boldsymbol{\mu}_0))$ and $\boldsymbol{B}(\boldsymbol{q}(\boldsymbol{x};\boldsymbol{\mu}_0)) \approx \tilde{\boldsymbol{B}}(\boldsymbol{x};\boldsymbol{\eta}(\boldsymbol{\mu}_0))$. Due to this approximation, one cannot expect these vector fields to vanish exactly on their respective domains. Instead, we recast the given problem as the following optimization problem:

$$\min_{\boldsymbol{\eta}} \left\| \tilde{\boldsymbol{R}}(\cdot;\boldsymbol{\eta}(\boldsymbol{\mu}_0)) \right\|_{\Omega} \quad \text{subject to} \left\| \tilde{\boldsymbol{B}}(\cdot;\boldsymbol{\eta}(\boldsymbol{\mu}_0)) \right\|_{\delta} < \epsilon. \tag{3}$$

Here, ϵ denotes a suitable tolerance specified for approximately satisfying the boundary conditions. The literature [2, 14, 15] recommends using the $\mathscr{L}^1$ norm in the cost function and constraint over the respective ranges Ω and δ. The 'truth' FOM for our problem is the steady Reynolds-averaged Navier Stokes (RANS) equation set with a suitable turbulence model. However, the residual is conveniently evaluated using the Euler equations since the lower order POD modes encapsulate global structures that cannot resolve finer near-wall details, but they do already incorporate the viscous effects through the learning snapshots [2, 11, 13, 14, 16].

Omitted in the above description for the sake of brevity are several details like actual evaluation of the cost function, implementation of boundary conditions, and hyper-reduction; these may be found in Sinha et al. [11]. In particular, it is noted that hyper-reduction, where the residual is evaluated on a small sub-domain so as to effect the gains promised by ROM, is not pursued here due to the chosen simplicity of the 2D problem.

B. Transported snapshot model order reduction (TSMOR)

Nair and Balajewicz [5] proposed this nonlinear modal decomposition approach for shock-dominated flows. As in the POD-ROM approach, TSMOR also comprises an offline stage and an online stage. Below, we briefly outline the method; the remaining details may be found in the original work, as well as in previous work from our group [6].

1. Offline stage

The offline stage is a one-time process that involves the computation of a database of flow 'snapshots' spanning a sufficiently rich parameter space, as well as the determination of their respective 'transport fields'. The latter are used for the approximation of the flow field for new parameters in the online stage.

The transport field corresponding to the j^{th} snapshot is denoted as $\boldsymbol{\xi}(\boldsymbol{x};\boldsymbol{\mu}_j,\boldsymbol{\mu})$, whose component in the i^{th} coordinate direction is ξ_i. It is computed such that the transported snapshot is able to approximately reconstruct the other snapshots in its neighborhood in parameter space. The very first step is to transport the grid as

$$\hat{\boldsymbol{x}}(\boldsymbol{x};\boldsymbol{\mu}_j,\boldsymbol{\mu}) \coloneqq \boldsymbol{x} + \boldsymbol{\xi}(\boldsymbol{x};\boldsymbol{\mu}_j,\boldsymbol{\mu}). \tag{4}$$

As the notation suggests, the transport is a function of the parameter vector of the snapshot being transported (i.e., $\boldsymbol{\mu}_j$) and the (neighbouring) parameter vector $\boldsymbol{\mu}$ whose solution needs to be approximated. The nature of the grid transport vector $\boldsymbol{\xi}$ is described subsequently. Now, the flow field corresponding to each grid point is taken to remain unchanged, even though the grid is transported; i.e., the flow field vector for the transported grid is denoted as

$$\hat{\hat{\boldsymbol{q}}}_j(\hat{\boldsymbol{x}}(\boldsymbol{x};\boldsymbol{\mu}_j,\boldsymbol{\mu})) \coloneqq \boldsymbol{q}(\boldsymbol{x};\boldsymbol{\mu}_j). \tag{5}$$

Once we have the flow solution defined on the transported grid, we interpolate/extrapolate $\hat{\hat{\boldsymbol{q}}}_j$ to the original undistorted grid:

$$\hat{\hat{\boldsymbol{q}}}_j(\hat{\boldsymbol{x}}(\boldsymbol{x};\boldsymbol{\mu}_j,\boldsymbol{\mu})) \xrightarrow[\text{extrapolation}]{\text{interpolation/}} \hat{\boldsymbol{q}}_j(\boldsymbol{x};\boldsymbol{\mu}). \tag{6}$$

where, $\hat{\boldsymbol{q}}_j(\boldsymbol{x};\boldsymbol{\mu})$ is the reference j^{th} snapshot transported and then interpolated/extrapolated to approximate the parameter vector $\boldsymbol{\mu}$ on the original grid.

Following Nair and Balajewicz [5], we write the i^{th} component of the transport field for the j^{th} snapshot as

$$\xi_i(\boldsymbol{x};\boldsymbol{\mu}_j,\boldsymbol{\mu}) = \sum_{m=1}^{N_{f,i}} \sum_{a=1}^{N_g} c_j^{i,m,a} f_{i,m}(\boldsymbol{x}) g_a(\boldsymbol{\mu}_j - \boldsymbol{\mu}). \tag{7}$$

One choice for the set of spatial basis functions $f_{i,m}$ are sinusoids with normalized coordinates as their arguments along with their harmonics, such that there are nodes/antinodes at certain salient points in the flow domain; see more in section III.D. On the other hand, the parameter basis functions g_a are typically multivariate polynomials. For example, one choice for the set of $N_g = 5$ bases when $\boldsymbol{\mu} = [M_\infty, \alpha]^T$ is

$$g(\boldsymbol{\mu}_j - \boldsymbol{\mu}) \in \{(M_{\infty j} - M_\infty), (\alpha_j - \alpha), (M_{\infty j} - M_\infty)^2, (M_{\infty j} - M_\infty)(\alpha_j - \alpha), (\alpha_j - \alpha)^2\}. \tag{8}$$

After the selection of the basis functions, the only unknowns in eqn. (7) are the coefficients c. Let $\boldsymbol{c}_j$ denote the set of all coefficients $c_j^{i,m,a}$ that have a common j (i.e., pertaining to one 'training' snapshot). The coefficients $\boldsymbol{c}_j$ are determined by minimizing the error (in the sense of the squared $\mathcal{L}_2$ norm) between the flow fields reconstructed by transporting the j^{th} snapshot to all its neighbouring snapshots in parameter space. Let N_t be the total number of such local neighboring snapshots chosen for the training. Then, one arrives at the following set of N_s independent optimization problems in the offline stage

$$\min_{\boldsymbol{c}_j} \frac{1}{N_t} \sum_{t=1}^{N_t} \left\| \hat{\boldsymbol{q}}_j(\boldsymbol{x};\boldsymbol{\mu}_t) - \boldsymbol{q}(\boldsymbol{x};\boldsymbol{\mu}_t) \right\|_2^2, \qquad \forall j \in \{1, 2, \ldots, N_s\}. \tag{9}$$

In the case of multidimensional parametric space, proper normalization of each parameter is a must prior to the determination of the neighborhood.

2. Online stage

As before, the online stage is concerned with the prediction of the flow solution at an unsampled parameter, say $\boldsymbol{\mu}_0$. The solution is approximated as a linear combination of local basis functions obtained by transporting the neighboring snapshots. Let N_v be the number of snapshots in the neighborhood of the $\boldsymbol{\mu}_0$ that are to be used in the reconstruction. Then, we have

$$\breve{\boldsymbol{q}}(\boldsymbol{x};\boldsymbol{\mu}_0) = \sum_{v=1}^{N_v} \zeta_v \hat{\boldsymbol{q}}_v(\boldsymbol{x};\boldsymbol{\mu}_0). \tag{10}$$

The only unknown is the vector of coefficients $\boldsymbol{\zeta} = [\zeta_1, \ldots, \zeta_{N_v}]^{\mathrm{T}}$. These are determined in a manner identical to online stage of the POD-ROM approach – i.e., by minimizing the residual of the governing equations subject to inequality constraints that approximate the boundary conditions.

C. Domain decomposition

The domain-decomposition approach outlined here is motivated by our work on the somewhat related problem of ROM for store-separation trajectory prediction [8]. Consider an airfoil in a transonic flow such that shocks exist only on one side (the suction side) of it. As shown in fig. 1, the overall flow domain Ω can be divided into two sub-domains:

- *Discontinuous flow sub-domain* (Ω_d): This is the maxinal region where a shock wave may be present across all the snapshots in a suitable parameter range. It is a simply-connected region without any 'holes'; it starts from above the airfoil surface and extends up to the height where the shock strength becomes negligible.
- *Continuous flow sub-domain* (Ω_c): This is the overall flow domain with a hole in it corresponding approximately to Ω_d (except for a small overlap region; see later).

Evidently, POD-ROM is applicable to Ω_c since the flow is smooth in it across the full range of parameters under consideration. On the other hand, Ω_d is amenable to TSMOR since a shock exists in here at all these parameters. We also identify a narrow overlap region (denoted as Ω_{cd}) between Ω_c and Ω_d. In the process, it is convenient to define two additional sub-domains. A 'basic' discontinuous flow sub-domain $\breve{\Omega}_d := \Omega_d - \Omega_{cd}$, and a 'basic' continuous flow sub-domain $\breve{\Omega}_c := \Omega_c - \Omega_{cd}$. Evidently, $\Omega = \breve{\Omega}_d + \breve{\Omega}_c + \Omega_{cd}$, the three being non-overlapping but contiguous.

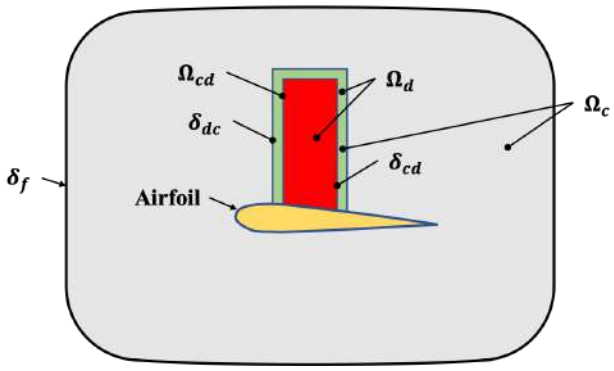

Fig. 1 Schematic of domain-decomposed approach for 2D transonic aerodynamics problem with shock on suction surface alone.

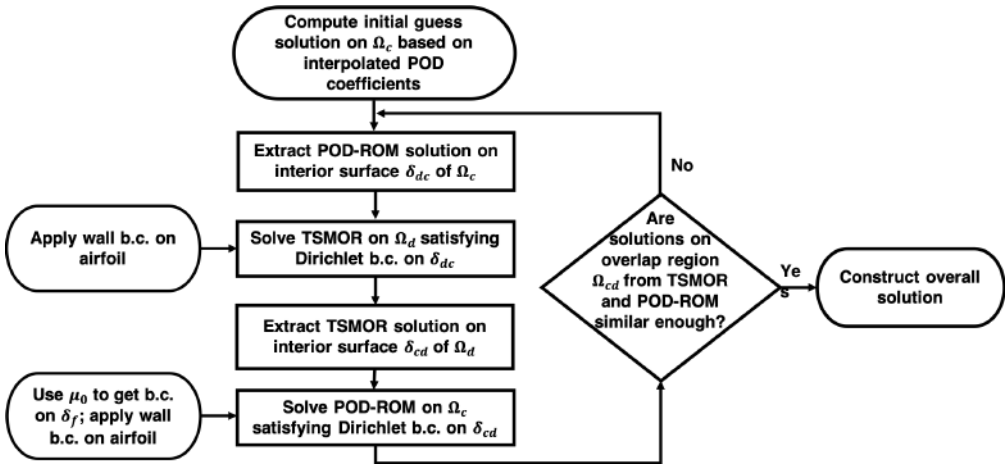

Fig. 2 Flow chart of steps involved in DDROM.

The actual domain-decomposed method is an iterative one; its flowchart is presented in fig. 2. A start is made by calculating the POD coefficients for the continuous flow sub-domain by interpolating the learning database over its parameter space. This yields the initial guess of the flow solution in Ω_c. From this, we extract the flow variables on the interior surface δ_{dc} that forms one of the boundaries of the discontinouos flow sub-domain Ω_d. This flow information now serves as the Dirichlet condition on the δ_{dc} boundary for the TSMOR method applied to Ω_d, apart from the no-slip condition at the airfoil wall. Once the TSMOR solution on Ω_d is in hand, we extract the flow variables on its interior surface δ_{cd}. Now, the POD-ROM is solved on Ω_c using the above information as the interfacing boundary condition on δ_{cd}, along with the far-field and airfoil wall boundary conditions. At this stage, we have the first iteration of the flow solutions on the overlap region Ω_{cd} from both the sub-domains. If these are too different, we can iterate the above procedure, starting again by extracting the flow variables on the interior surface δ_{dc} of Ω_c from the POD-ROM solution. On the other hand, if these are close enough, then we can cease iterating, and compose the overall solution. The reason for attempting the match the flow solutions on an overlap region of finite thickness rather than at a zero-thickness interface is to ensure (approximate) smoothness of the flow thereat apart from its (approximate) continuity.

The above description of the strategy pertains to cases where there is a single shock, say above an airfoil. However, the method can be easily extended to cases where there are multiple disjoint shocks, simply by having multiple discontinuous flow sub-domains correspondingly. TSMOR may be applied in each of these disjoint regions separately, and the flow solutions need to be matched at all of their interfaces with the remaining continuous flow sub-domain. An example of such an approach, albeit in the different context of store separation trajectory prediction, can be seen in our earlier work [8].

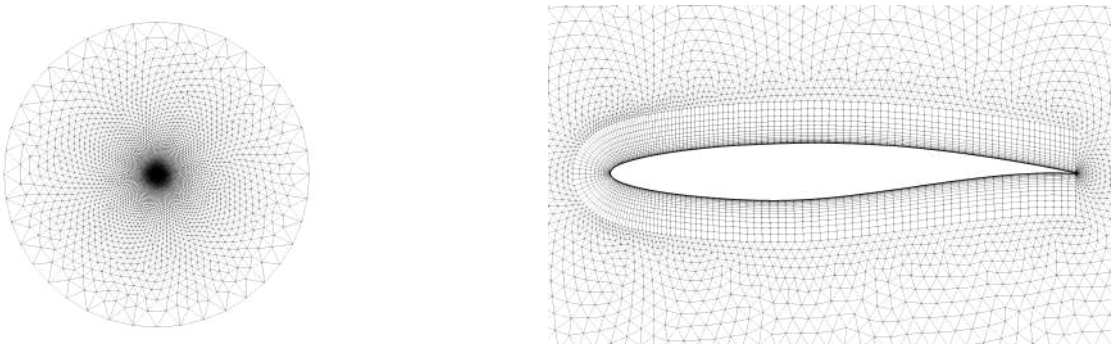

(a) (b)

Fig. 3 Topology of grid for the transonic airfoil (RAE 2822) flow problem adopted from Ref. [17]. (a) Full domain. (b) Zoomed view of body-fitted structured grid near the airfoil surface.

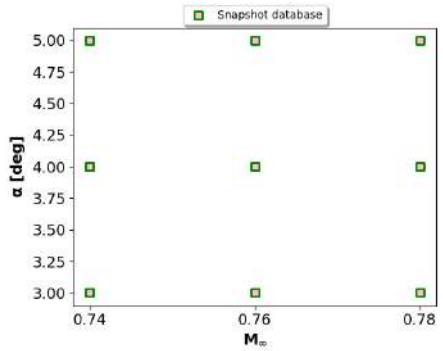

Fig. 4 Combinations of free-stream Mach number M_∞ and angle of attack α used for the learning database.

III. Results and discussion

A. Full-order model (FOM) database

We have implemented the proposed methodology on a two-dimensional transonic airfoil flow problem. The airfoil considered for the problem is the standard RAE 2822 geometry. Its chord c is used for non-dimensionalizing all length parameters. The flow domain and grid (see fig. 3) are taken from a test case of the open-source CFD software Stanford University Unstructured (SU2) [17], which also considers the same transonic flow problem albeit for a single parameter vector ($M_\infty = 0.729$, $\alpha = 2.31°$). The domain is circular with a radius of $100c$ centered at the leading edge of the airfoil. A structured 'C' type grid comprising of quadrilateral cells exists around the airfoil extending to about $0.1c$ from the surface, with the first grid point being at a distance of 1E-5c from the surface. The structured grid transitions to an unstructured grid of triangular cells. It has 13,937 nodes and 22,842 elements (18,042 triangles and 4,800 quadrilaterals), with 192 edges along the airfoil boundary and 40 along the far-field circle. We perform steady RANS calculations in SU2 [17, 18] using the Spalart-Almaras turbulence model. The freestream condition is enforced on the far-field boundary with a characteristics-based formulation; the airfoil surface is modelled as a no-slip adiabatic wall. The choice of the solver and its settings are retained from the SU2 test case [17].

Figure 4 depicts the nine $M_\infty - \alpha$ combinations chosen for the learning database generation. In all these cases, there is a shock on the suction side of the airfoil only.

The flow variable vector extracted from the solution is $\boldsymbol{q} = [\rho, \rho u, \rho v, p]^{\mathrm{T}}$, as mentioned before. That is, although RANS calculations were performed, Euler variables were used in the ROM for reasons mentioned in section II. Density is non-dimensionalized by the freestream density – ρ_∞, velocity is non-dimensionalized by the freestream speed of sound $a_\infty = \sqrt{\gamma p_\infty / \rho_\infty}$, where γ is the ratio of specific heats of air and p_∞ is the freestream pressure. Pressure is non-dimensionalized by $\rho_\infty a_\infty^2 = \gamma p_\infty$, so that the non-dimensional freestream pressure is $1/\gamma$.

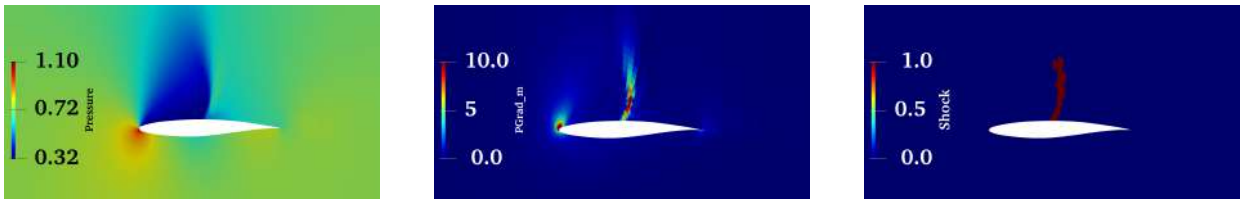

(a) $M_\infty = 0.74$, $\alpha = 5°$: pressure (b) $M_\infty = 0.74$, $\alpha = 5°$: $\|\nabla p\|$ (c) $M_\infty = 0.74$, $\alpha = 5°$: shock region

(d) $M_\infty = 0.78$, $\alpha = 3°$: pressure (e) $M_\infty = 0.78$, $\alpha = 3°$: $\|\nabla p\|$ (f) $M_\infty = 0.78$, $\alpha = 3°$: shock region

Fig. 5 Pressure, pressure gradient magnitude and identified shocked regions in two representative cases.

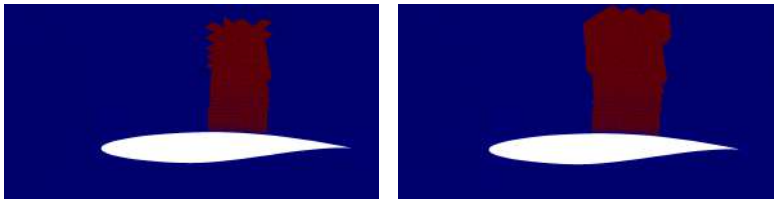

(a) (b)

Fig. 6 (a) The basic discontinuous flow sub-domain $\breve{\Omega}_d$ that is the convex hull of all shocked cells across all the learning snapshots. (b) The discontinuous flow sub-domain Ω_d formed by adding to $\breve{\Omega}_d$ the overlap region Ω_{cd} comprising of one layer of cells from the continuous flow sub-domain Ω_c.

B. Identifying the discontinuous flow sub-domain

A shock is a thin region displaying large changes in all flow properties, including pressure. Figures 5(a) and 5(d) show the pressure fields in two representative cases – where the shock is at its most upstream and downstream positions respectively. We compute the magnitude of the pressure gradient at all grid cells (using the values of pressure stored at all their vertices). Corresponding to the above pressure fields, the pressure gradient magnitude fields are presented in Figures 5(b) and 5(e), respectively. Apart from the shock region, the areas near the leading stagnation point and the trailing edge also have high pressure gradients. Moreover, due to boundary layer effects, the foot of the shock at the airfoil surface does not display very high gradients. To identify the shock-containing cells, a non-dimensional pressure gradient magnitude threshold of 3.0 is arrived at by trial and error. An additional constraint is applied – viz. cells with $\|\nabla p\| > 3.0$ should also have their centroidal x-coordinate sufficiently away from both 0 and 1, so as to avoid the leading and trailing edge regions. Finally, the region identified thus is algorithmically extended to the airfoil surface using the facts that (a) the region is above the airfoil, and (b) the grid comprises of only quadrilateral cells in this area. Figures 5(c) and 5(f) demonstrate that this strategy is able to identify the shock region distinctly in both cases.

Once we have identified the cells comprising the shock regions corresponding to all nine snapshots, the 'basic' discontinuous flow sub-domain $\breve{\Omega}_d$ is constructed as their convex hull using a standard algorithm. Figure 6(a) depicts this for the considered parameter range. Next, we have to expand $\breve{\Omega}_d$ to form the overlap region Ω_{cd}, whose union will make it the 'final' discontinuous flow sub-domain Ω_d. For this, we wish to identify at least one layer of cells immediately 'outside' $\breve{\Omega}_d$. To do so, we first identify the continuous flow domain Ω_c as $\Omega - \breve{\Omega}_d$, and especially the interface of the two viz. δ_{cd}. Then, the overlap region Ω_{cd} is formed by all the cells in Ω_c that have at least one node in common with δ_{cd}. Addition of Ω_{cd} to $\breve{\Omega}_d$ yields the discontinuous flow sub-domain Ω_d that is depicted in fig. 6(b).

Custom programs are developed in-house in Python for these mesh manipulations, as well as for arriving at all the

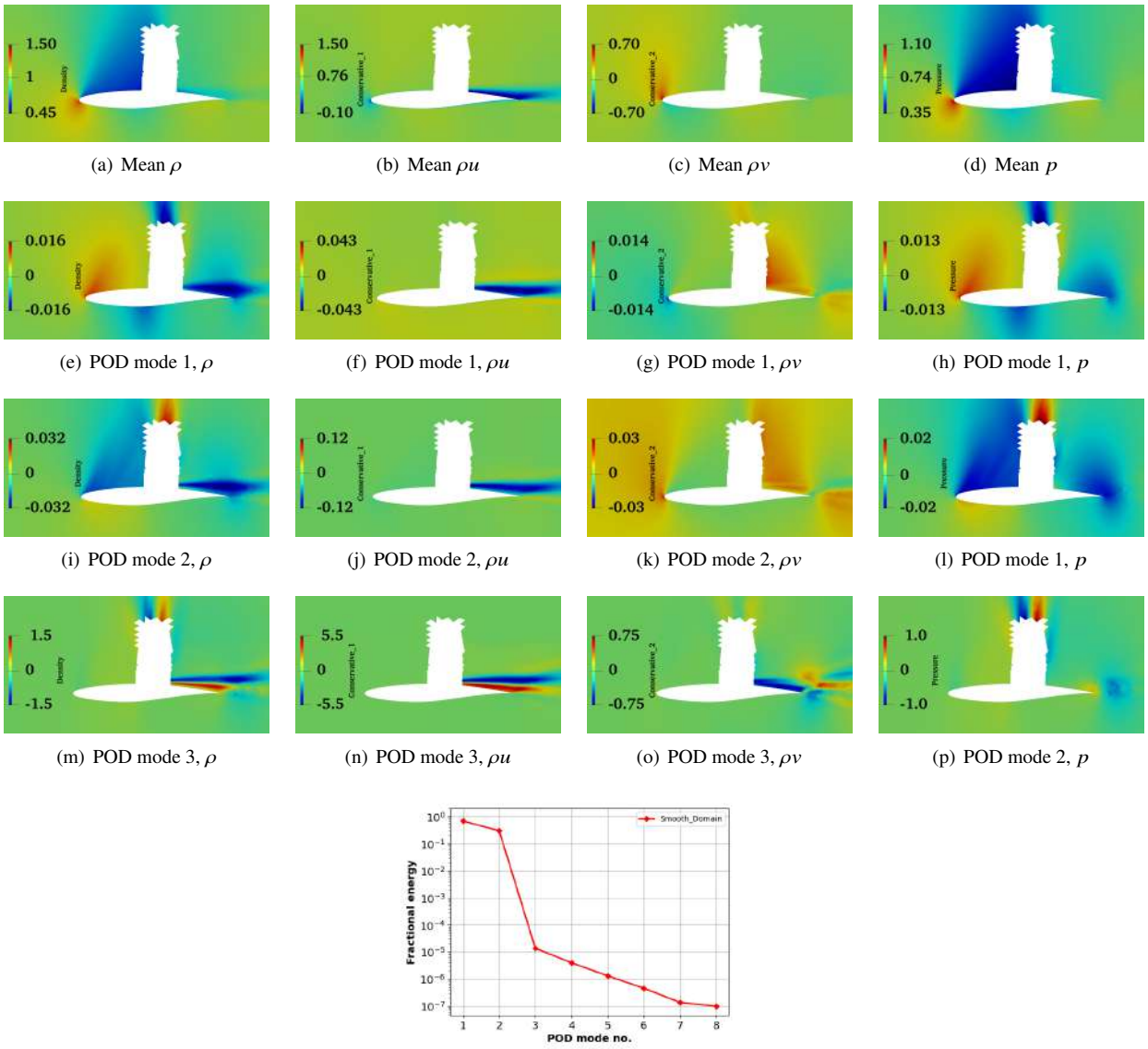

(a) Mean ρ (b) Mean ρu (c) Mean ρv (d) Mean p

(e) POD mode 1, ρ (f) POD mode 1, ρu (g) POD mode 1, ρv (h) POD mode 1, p

(i) POD mode 2, ρ (j) POD mode 2, ρu (k) POD mode 2, ρv (l) POD mode 1, p

(m) POD mode 3, ρ (n) POD mode 3, ρu (o) POD mode 3, ρv (p) POD mode 2, p

(q) POD eigenspectrum

Fig. 7 Results from proper orthogonal decomposition performed on the continuous flow sub-domain Ω_c.

results discussed below.

C. POD results

The results from POD performed on the continuous flow sub-domain Ω_c are presented in fig. 7. The average from the learning database has freestream Mach number of approximately 0.76 and angle of attack of approximately 4°. These are apparent in the x- and y-momenta components far from the airfoil. Moreover, the average pressure (and density) fields show the presence of the (average) shock in the lowering of static pressure (and density) in a pocket over the suction surface.

The fractional modal 'energy' is defined as $\lambda^{(n)}/\sum_{n'} \lambda^{(n')}$; it gives the relative prevalence of the respective POD modes in the database. Evidently, there is a large separation in 'energy' between the first two POD modes, and all the rest. This is unsurprising since the first two POD modes account for the major flow variations in the overall Ω_c sub-domain (as discussed below), whereas the higher-order POD modes encode the near-surface small-scale flow structures.

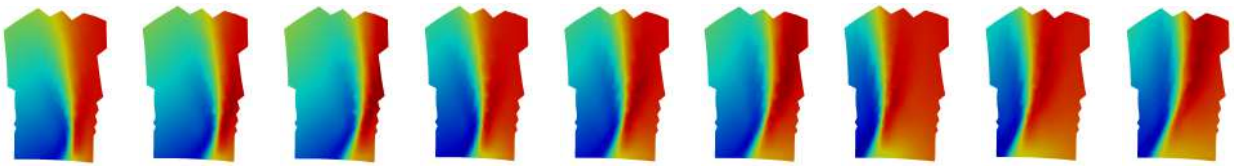

(a) 0.74, 3° (b) 0.76, 3° (c) 0.78, 3° (d) 0.74, 4° (e) 0.76, 4° (f) 0.78, 4° (g) 0.74, 5° (h) 0.76, 5° (i) 0.78, 5°

Fig. 8 Pressure fields in the discontinuous flow sub-domain for all the nine cases in the learning database indicated by their respective M_∞, α pairs. Consistent color levels are used, distributed between 0.3 and 0.7.

Indeed the x-momentum component of the first POD mode presents an almost uniform positive value away from the airfoil surface corresponding to the M_∞ variations (specifically increments in M_∞) in the database. The corresponding decrease in suction near the leading edge is apparent in the pressure field. Moreover, the consequent aft movement of the shock causes the negative pressure band at the head of the shock region. Conversely, the other major variation in the database, viz. in angle of attack, is captured by the second POD mode. This is apparent in its positive values of ρv away from the airfoil corresponding to increases in α. Such increases causes the shock to move forward, which results in the corresponding increase in suction and a positive pressure band at the head of the shock region.

The higher-order POD modes (i.e., POD mode 3 and onward) cannot be interpreted as crisply. The presence of the shock at various positions in the database leaves a more confusing imprint in these modes, as is apparent from figs. 7(m)–7(p). However, inclusion of them in the subsequent reduced order models allows the continuation of the shocked solution from the discontinuous flow sub-domain.

D. Details of the TSMOR implementation specific to the problem

The variation of the pressure field in the discontinuous flow sub-domain Ω_d across the nine cases in the learning database is shown in fig. 8. This clearly shows the kind of movement and strength changes incurred by the shock in the database. An understanding of these modifications informs the choice of the grid transport spatial basis functions $f_{i,m}(\boldsymbol{x})$ in eqn. (7).

Let the overall streamwise and cross-stream extents of the Ω_d sub-domain be denoted by L_x and L_y, respectively. Clearly, $L_x = \max_{\Omega_d} x - \min_{\Omega_d} x$, and L_y is also likewise. Further, let us define the scaled and shifted x- and y-coordinates as $x' := \left(x - \min_{\Omega_d} x\right)/L_x$ and $y' := \left(y - \min_{\Omega_d} y\right)/L_y$. Evidently, both x' and y' are in the range $[0, 1]$.

The shock moves upstream and downstream, which necessitates a bodily transport of the snapshots in the x-direction. This can be effected by choosing one of the x-transport bases as unity. The shock-affected region can get compressed or extended in the x-direction, for which we include a $\sin(\pi x')$ basis. Other possible 'wrinkling' modes may be accounted for by generally choosing x-direction transport bases of the form $\sin(n\pi x')$ for $n \in \mathbb{N}$. These bases, called 'self' terms, result in same x-transport at all y-coordinates. However, one can observe significant changes in the obliqueness of the shock as well as in its curvature. These may be accommodated with 'cross' terms in the x-transport bases of the form $\sin(m\pi y'/2)$ for $m \in \mathbb{N}$. Note that the $m = 1$ term may cause the shock to lean downstream, whereas the $m = 2$ term may cause it to bulge out.

Changes of the shock in the cross-stream direction are mainly in its height. This can be effected by choosing 'self' terms in the y-transport bases of the form $\sin(\pi y'/2)$. Higher order harmonics of this may be included to allow greater flexibility in modelling localized distortions. Finally, a unity basis may be included to allow a bodily movement, howsoever slight, which may be ameliorated in the subsequent extrapolation step. 'Cross' terms do not appear to be necessary in the y-transport bases, as changes in the obliqueness may be equivalently effected by the cross terms in x-transport bases.

Based on the above discussion, the following choice is made for the spatial basis functions of the grid transport:

$$f_1(x,y) \in \underbrace{\{1, \sin\pi x', \sin 2\pi x', \ldots, \sin(N_{xx}-1)\pi x'\}}_{N_{xx}\text{ elements}} + \underbrace{\{\sin\pi y'/2, \sin 2\pi y'/2, \ldots, \sin N_{xy}\pi y'/2\}}_{N_{xy}\text{ elements}}, \tag{11a}$$

$$f_2(x,y) \in \underbrace{\{1, \sin\pi y'/2, \sin 2\pi y'/2, \ldots, \sin(N_{yy}-1)\pi y'/2\}}_{N_{yy}\text{ elements}}. \tag{11b}$$

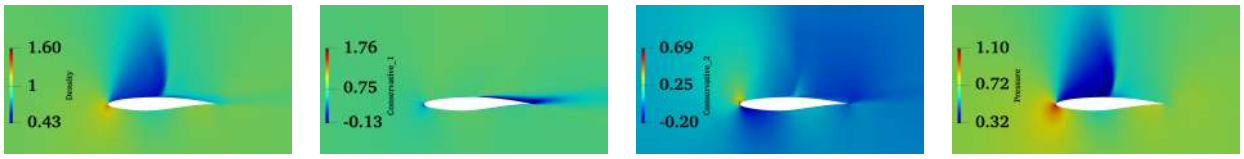

(a) Predicted ρ (b) Predicted ρu (c) Predicted ρv (d) Predicted p

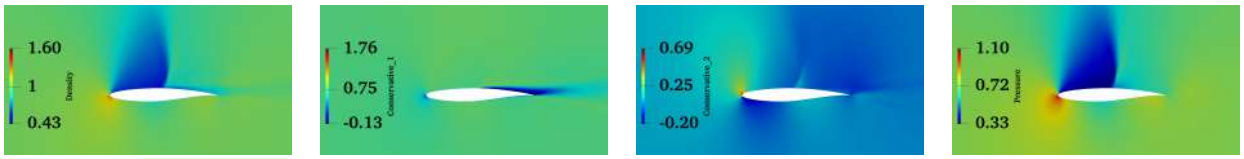

(e) Truth ρ (f) Truth ρu (g) Truth ρv (h) Truth p

Fig. 9 (a)-(d) ROM prediction and (e)-(h) 'truth' flow solutions' components at $M_\infty = 0.75$, $\alpha = 4.5°$.

Table 1 Quantitative verification of proposed domain-decomposed MOR approach.

Case		c_l			$c_d \times 10$			$c_{m,c/4} \times 10$		
M_∞	α	Truth	MOR	% Error	Truth	MOR	% Error	Truth	MOR	% Error
0.77	4.5°	0.7545	0.7547	0.02	0.544	0.547	0.53	0.928	0.924	0.45
0.75	4.5°	0.840	0.800	4.77	0.488	0.499	2.18	0.901	0.820	9.00
0.77	3.5°	0.716	0.790	10.30	0.416	0.490	17.60	1.000	0.821	17.90
0.75	3.5°	0.817	0.794	2.80	0.35	0.420	19.00	0.990	0.840	15.15

Preliminarily, we have used $N_{xx} = 3$, $N_{xy} = 2$, and $N_{yy} = 3$; we intend to optimize this subsequently.

E. Verification of DDROM

We bring everything together in a verification assay. In particular, we assess the ability of our proposed MOR in predicting the flow field for a new parameter vector that is not in the learning database, but is in its range, viz. $M_\infty = 0.75$, $\alpha = 4.5°$. Figure 9 demonstrates that our predictions are essentially indistinguishable from the 'truth' solution obtained by solving the full-order model (FOM) (i.e., RANS simulations) in SU2.

A more quantitative assessment of the performance of our proposed MOR is pursued now. We calculate the lift, drag and pitching moment coefficients (about the quarter-chord point) from the predicted flow field vector, and compare these with their truth counterparts. Moreover, we extend the analysis to more test cases. The results, presented in table 1, attest to the encouraging overall performance of the proposed MOR approach.

However, we also notice some areas of concern. The pitching moment typically has more errors compared to the lift and drag, owing to its greater sensitivity to the flow field. The drag coefficient is not predicted with sufficient accuracy for the two $\alpha = 3.5°$ cases. Prediction of lift is somewhat more consistent and accurate. Several avenues may be explored in the future for improving these results. Firstly, the discontinuous flow sub-domain Ω_d may be enlarged to reduce the burden on the POD-ROM applied to the continuous flow sub-domain Ω_c, given that the head of the shock is going outside Ω_d (see fig. 8). The grid transport's spatial bases may be enriched with terms that afford greater distortion. For example, a direct term of the form $\sin \pi x'/2$ in the x-transport will allow differential transport of the upstream and downstream extremities of Ω_d. Finally, a hyper-reduction strategy may be adopted in the online stages of both POD-ROM and TSMOR to reduce the burden on the associated optimization.

IV. Conclusion

We propose a novel reduced-order model (ROM) strategy for shock-dominated flows that decomposes the flow domain Ω into a discontinuous flow sub-domain Ω_d and a continuous flow sub-domain Ω_c. This decomposition is empirical and automatic. The former sub-domain contains the shock under all parametric conditions, and transported

snapshot model order reduction (TSMOR) is applied to it. The latter sub-domain, as its name suggests, is designed to be devoid of discontinuities under all parametric conditions, and POD-based ROM is used in it. The solutions in the two sub-domains are to be matched at the interface in an iterative manner. Since both ROMs are inexpensive individually, a few iterations of them should still deliver significant savings compared to the full-order model (FOM) solution approach (which is RANS simulation in the present instance).

The method is applied to a transonic airfoil aerodynamics problem. Steady RANS simulations are performed at nine combinations of free-stream Mach number and angle of attack, all pertaining to transonic flow with the shock existing over the suction surface alone. We demonstrate the algorithmic identification of the Ω_d sub-domain by thresholding based on the magnitude of pressure gradient in the flow snapshots, together with the imposition of some additional conditions. We also describe the automatic generation of the learning database for TSMOR on Ω_d from the overall flow database. Finally, we present results from the overall domain-decomposed MOR strategy, showing encouraging agreement with the truth solution.

Future work in this regard will center upon improvements to the procedure as outlined in the text. Moreover, the method needs to be extended to be able to address the presence of shocks over both the suction and pressure surfaces. Finally, the ultimate goal of this research endeavour is to address realistic three-dimensional problems of transonic aerodynamics.

References

[1] Lucia, D., King, P., Oxley, M., and Beran, P., "Reduced order modeling for a one-dimensional nozzle flow with moving shocks," *15th AIAA computational fluid dynamics conference*, 2001.

[2] Alonso, D., Vega, J., and Velazquez, A., "Reduced-order model for viscous aerodynamic flow past an airfoil," *AIAA journal*, Vol. 48, No. 9, 2010, pp. 1946–1958.

[3] Carlberg, K., Choi, Y., and Sargsyan, S., "Conservative model reduction for finite-volume models," *Journal of Computational Physics*, Vol. 371, 2018, pp. 280–314.

[4] Abgrall, R., and Crisovan, R., "Model reduction using L 1-norm minimization as an application to nonlinear hyperbolic problems," *International Journal for Numerical Methods in Fluids*, Vol. 87, No. 12, 2018, pp. 628–651.

[5] Nair, N. J., and Balajewicz, M., "Transported snapshot model order reduction approach for parametric, steady-state fluid flows containing parameter-dependent shocks," *International Journal for Numerical Methods in Engineering*, Vol. 117, No. 12, 2019, pp. 1234–1262.

[6] Goyal, M., and Sinha, A., "Transported Snapshot Model Order Reduction for Steady Transonic Flows Simulated On Unstructured Meshes," *AIAA SCITECH 2023 Forum*, 2023.

[7] Sinha, A., and Garg, S., "Reduced-order modeling of steady aerodynamics for 2D store separation analysis," *2018 Applied Aerodynamics Conference, AIAA Paper 3168*, 2018.

[8] Pandey, N., Tembhare, R., Singh, N., and Sinha, A., "Domain-decomposed reduced-order modelling of steady aerodynamics for 2D store separation analysis," *AIAA Scitech Forum, AIAA Paper 1004*, 2023.

[9] Lumley, J. L., "The structure of inhomogeneous turbulent flows," *Atm. Turb. and Radio Wave Prop.*, edited by A. M. Yaglom and V. I. Tatarsky, Nauka, Moscow, 1967, pp. 166–178.

[10] Holmes, P., Lumley, J. L., Berkooz, G., and Rowley, C. W., *Turbulence, Coherent Structures, Dynamical Systems and Symmetry*, Cambridge University Press, 2012.

[11] Sinha, A., Kumar, R., and Umakant, J., "Reduced-order model for efficient generation of a subsonic missile's aerodynamic database," *The Aeronautical Journal*, Vol. 126, 2022, pp. 1546–1567.

[12] LeGresley, P., and Alonso, J. J., "Investigation of non-linear projection for pod based reduced order models for aerodynamics," *39th AIAA Aerospace Sciences Meeting and Exhibit, paper 926*, 2001.

[13] Zimmermann, R., and Görtz, S., "Non-linear reduced order models for steady aerodynamics," *Procedia Computer Science*, Vol. 1, 2010, pp. 165–174.

[14] Alonso, D., Vega, J., Velazquez, A., and Pablo, V., "Reduced-order modeling of three-dimensional external aerodynamic flows," *Journal of Aerospace Engineering*, Vol. 25, 2012, pp. 588–599.

[15] Alonso, D., Velazquez, A., and Vega, J. M., "A method to generate computationally efficient reduced order models," *Computer Methods in Applied Mechanics and Engineering*, Vol. 198, 2009, pp. 2683–2691. https://doi.org/10.1016/j.cma.2009.03.012.

[16] Zimmermann, R., and Görtz, S., "Improved extrapolation of steady turbulent aerodynamics using a non-linear POD-based reduced order model," *Aeronautical Journal*, Vol. 116, No. 1184, 2012, pp. 1079–1100.

[17] Palacios, F., Economon, T. D., Aranake, A. C., Copeland, S. R., Lonkar, A. K., Lukaczyk, T. W., Manosalvas, D. E., Naik, K. R., Padrón, A. S., Tracey, B., Variyar, A., and Alonso, J. J., "Stanford University Unstructured (SU2): Open-source analysis and design technology for turbulent flows," *52nd AIAA Aerospace Sciences Meeting, paper 0243*, 2014.

[18] Palacios, F., Colonno, M. R., Aranake, A. C., Campos, A., Copeland, S. R., Economon, T. D., Lonkar, A. K., Lukaczyk, T. W., Taylor, T. W. R., and Alonso, J. J., "Stanford University Unstructured (SU2): An open-source integrated computational environment for multi-physics simulation and design," *51st AIAA Aerospace Sciences Meeting, paper 0287*, 2013.